SARS-CoV-2 infection activating a novel variant of the *NOTCH3* gene and subsequently causing development of CADASIL

Zbigniew J. Król[1], Małgorzata Dorobek[1], Maciej Dąbrowski[2], Justyna Zielińska-Turek[1],
Bartosz Mruk[3], Jerzy Walecki[3], Katarzyna Sklinda[3], Robert Gil[1], Agnieszka Pawlak[1],
Marzena Wojtaszewska[2], Adrian Lejman[2], Paula Dobosz[2], Paweł Zawadzki[2], Aneta Pawłowska[1],
Michał Szczepaniak[1], Dorota Król[1], Artur Zaczyński[1], Waldemar Wierzba[1]

[1]Central Clinical Hospital of the Ministry of Interior and Administration, Warsaw, Poland
[2]MNM Diagnostic, Poland
[3]Department of Radiology, Centre of Postgraduate Medical Education, Warsaw, Poland

Corresponding author:
Prof. Waldemar Wierzba
Central Clinical
Hospital of the
Ministry of Interior
and Administration
Warsaw, Poland
E-mail: waldemar.wierzba@
cskmswia.gov.pl

Abstract

Introduction: In the following study we describe the diagnostic process and further case analysis of a 30-year-old woman admitted with typical COVID-19 symptoms, who subsequently developed additional symptoms suggesting cerebral autosomal dominant arteriopathy with sub-cortical infarcts and leukoencephalopathy (CADASIL).
Material and methods: Other than the standard diagnostic procedures, whole genome sequencing (WGS) was used, which led to following findings. A new variant of the *NOTCH3* gene, which led to CADASIL-like symptoms, was found, and it had been most likely activated by the SARS-CoV-2 infection. This novel variant in NOTCH3 has not been found in existing databases and has never been mentioned in research concerning CADASIL before.
Results: Furthermore, after subjecting the patient's close relatives to WGS it was found that no other examined person demonstrated the same genetic mutation.
Conclusions: It seems therefore that the new variant of *NOTCH3* is of *de novo* origin in the patient's genome. Additionally, the relatively early onset of CADASIL and the unexpectedly severe COVID-19 infection suggest that the two occurred simultaneously: the infection with SARS-CoV-2 accelerated development of CADASIL symptoms and the unusual variant of the *NOTCH3* gene contributed to the more severe course of COVID-19.

Key words: SARS-CoV-2, COVID-19, encephalitis, CADASIL, whole genome sequencing, *NOTCH3* gene.

Introduction

Encephalopathy and stroke in COVID-19 patients have been repeatedly reported [1–5]. Previous reports indicate that SARS-CoV-2 infection is associated with a significantly escalated risk of ischaemic stroke, especially with potential cryptogenic stroke. The incidence of ischaemic stroke in the context of COVID-19, according to various reports, varies between 2.5% and 6.4%, but may be higher [1]. Instances of strokes comorbid

AMS

Z.J. Król, M. Dorobek, M. Dąbrowski, J. Zielińska-Turek, B. Mruk, J. Walecki, K. Sklinda, R. Gil, A. Pawlak, M. Wojtaszewska, A. Lejman, P. Dobosz, P. Zawadzki, A. Pawłowska, M. Szczepaniak, D. Król, A. Zaczyński, W. Wierzba

with COVID-19 are characterised by the patients' lower than average age, large vessel occlusion, possible antiphospholipid antibody production, raised inflammatory markers, concomitant venous thromboembolism and multi-territory infarcts. Additionally, preceding vascular comorbidities are frequently observed, and the incidence of stroke increases with COVID-19 severity [4, 6–8].

Encephalopathy is also present in cerebral autosomal dominant arteriopathy with subcortical infarcts and leukoencephalopathy (CADASIL). CADASIL is the most common monogenic vascular disease which causes young-adult onset of cerebrovascular disease. The definitive diagnosis of CADASIL is based on sequencing the *NOTCH3* gene, as it results from pathogenic, loss-of-function mutations in this specific gene [9, 10]. The primary pathology is the accumulation of abnormal transmembrane deposits on vascular smooth muscle cells in the brain and other organs [11]. This leads to impaired vascular function, resulting in recurrent ischaemic incidents that manifest with migraine with aura, transient ischaemic attacks or strokes and dementia before the age of 60 [12]. CADASIL has a gradual and progressive course in younger patients, who are often free from classical vascular risk factors.

Hereby we present a case of a 30-year-old patient with COVID-19 and mild systemic biochemical signs of inflammation associated with leukoencephalopathy, which was finally diagnosed as CADASIL.

Case report – COVID-19 patient

A 30-year-old woman with a history of allergic reaction, spastic right sided hemiparesis and paresis of the right abduction nerve (neurologic deficit present from the age of two, never radiologically diagnosed) was diagnosed with SARS-CoV-2 infection with reverse transcription polymerase chain reaction (RT-PCR) of nasopharyngeal swab. The patient was free of vascular risk factors.

The onset of the infection started with temperature elevated to 37°C. Three days after the initial symptoms the patient complained of a swollen tongue, anosmia and general weakness. On the 11th day of the illness the patient was admitted to an emergency department with right-sided pulsating headache, dysarthria, fatigue and psychomotor slowness. The patient's general condition was good, and oxygen saturation and blood pressure were normal. Leucocytosis grew to 15.7 thousand/μl. The remaining biochemical tests and cerebrospinal fluid (CSF) were normal. Microbiological tests ruled out the presence of bacteria in urine, faeces and blood.

Chest CT revealed small peripheral areas of ground glass opacities in the lower segments of both lungs (3.16% lung surface occupancy).

Intravenous treatment with ceftriaxone and acyclovir was commenced, regardless of which on the 3rd day of treatment the patient's consciousness deteriorated and neck stiffness occurred. CSF for JC virus and SARS-CoV-2 virus was negative. CSF was also negative for bacteria. The levels of class G immunoglobulins were elevated and measured at three times higher than regular values. No oligoclonal bands were present. Infection with hepatitis B virus (HBV), hepatitis C virus (HCV), respiratory syncytial virus (RSV) and influenza viruses in serum was ruled out.

The patient had been administered intravenous immunoglobulins, 30 g/day, for 3 days. During the following days impaired consciousness and dysarthria deepened, and neck stiffness was still present. Convalescent plasma was given on the 20th and 21st day (1 unit per day) when the first neurological symptoms occurred. Blood samples were collected before and after plasma administration in order to assess the inflammatory parameters. After convalescent plasma transfusion increases in IL-2, IL-8 and TNF-α were observed whereas IL-15 was decreased (Table I). Moreover, the concentrations of other cytokines (IL-1a, IL-1b, IL-4, IL-6, IL-10, IL-12, IL-17, IL-23, INF-γ, TNF-β) did not change.

After transfusion of convalescent plasma, the patient's neurological condition improved [13]. Within 12 days of admission to the hospital clinical symptoms subsided. Follow-up CT of the lungs revealed no pathology. Anosmia disappeared, and speech returned to normal. Slowness, general weakness and sleepiness also ceased.

At discharge and during follow-up visits (1 to 6 months after hospitalization) on neuropsychologic examination, discrete weakening of the concentration, attention, direct memory and executive functions was still present. There was no cognitive dysfunction, but the tendency of reduced mood was observed. The patient reported depression, general weakness, fatigue and right-sided migraine-like headaches, which gradually disappeared.

Table I. Levels of cytokine and glucose-6-phosphate dehydrogenase before and after plasma transfusion of convalescents (pg/ml)

Parameter	IL-2	IL-8	IL-15	TNF-α
Levels before	30.60	22.94	28.10	< 17.28
Levels after	40.19	38.58	< 26.88	39.09

The process leading to CADASIL diagnosis

Neuro-radiologic data

The first MRI scans of the brain were performed on the 12th day of the infection and as soon as neurological symptoms began. They revealed the presence of multiple, at least a dozen, hyperintense foci in T2 WI and FLAIR, which were located in the white matter of both hemispheres (frontal, parietal and temporal lobes were affected), with the most prominent lesions situated symmetrically close to the lateral ventricles, and a single one in the knee of the corpus callosum. Some of the foci presented nodular contrast enhancement and diffusion restriction on DWI 9 (Figures 1, 2). There were no infratentorial lesions. MRI of the cervical spine was normal. Apart from these lesions, a small subdural haematoma of the right hemisphere was present, but there were no intraparenchymal microhaemorrhages. Meningeal thickening and contrast enhancement of the right hemisphere were present.

Subsequent control MRI scans of the brain (13.08, 20.08.2020) showed white matter changes within the cerebral hemispheres without significant dynamics, i.e., the location and morphology. The sizes of the lesions were of similar volume with slight contrast enhancement (Figure 2).

The follow-up MRI examination (3.09.2020) revealed the lesions which showed slight diffusion restriction on DWI and discrete contrast enhancement. Meningeal thickness was no longer present.
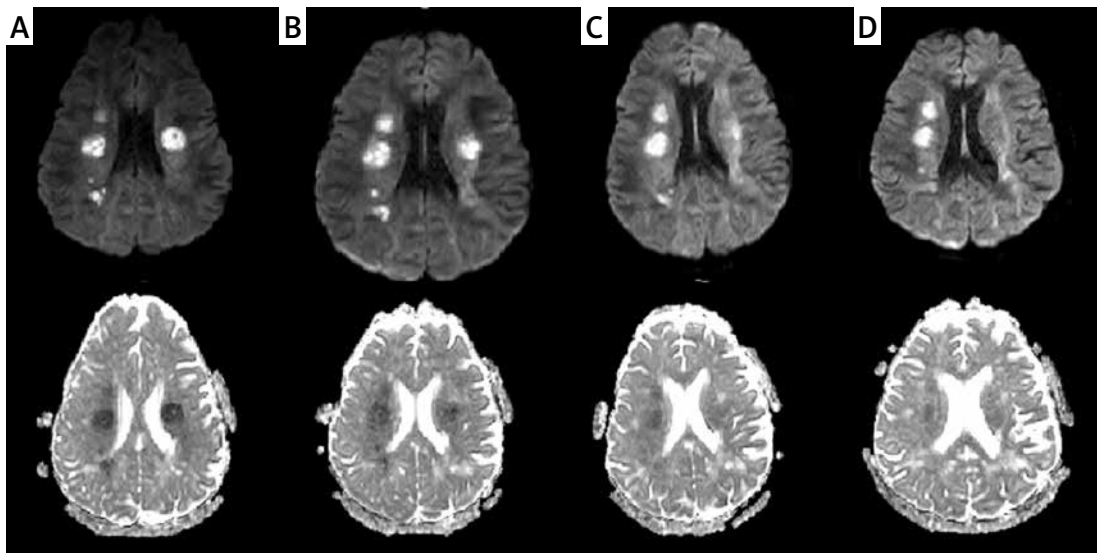
Figure 1. Magnetic resonance imaging of the brain on admission 5/08 (**A**) and the dynamics of changes in the control examinations 8/08 (**B**), 13/08 (**C**), 20/08 (**D**)
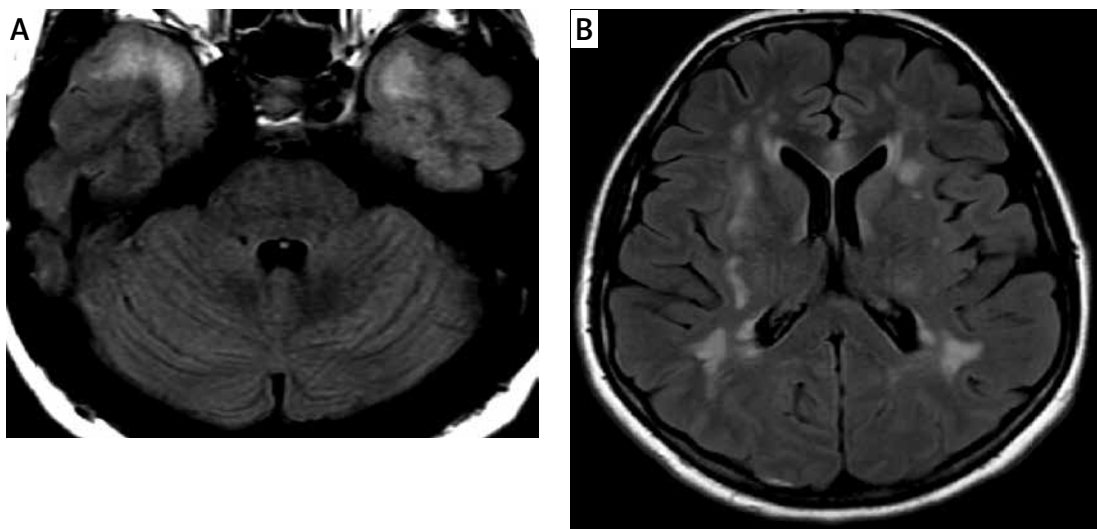
Figure 2. FLAIR image (**A**) shows confluent hyperintensities within the white matter of the anterior temporal poles. FLAIR image at the level of lateral ventricles (**B**) demonstrates white matter changes within the external capsules (mainly on the right)

Z.J. Król, M. Dorobek, M. Dąbrowski, J. Zielińska-Turek, B. Mruk, J. Walecki, K. Sklinda, R. Gil, A. Pawlak, M. Wojtaszewska, A. Lejman, P. Dobosz, P. Zawadzki, A. Pawłowska, M. Szczepaniak, D. Król, A. Zaczyński, W. Wierzba

The last follow-up examination (05.11.2020) showed the same number of lesions, showing no diffusion restriction on DWI or enhancement after gadolinium-based contrast administration.

Genetic data – whole genome sequencing

Considering the fact that in March 2020 the hospital was transformed into a unit handling solely COVID-19 patients, the opportunity arose to participate in projects related to broadening the knowledge about the disease and improving the care patients can receive. One of those ongoing projects focuses on genetic factors contributing to the severity of COVID-19 and potential immunity. The patient agreed to participate in the study and therefore whole genome sequencing (WGS) was applied, which allowed identification of the genetic background of neurological symptoms.

The patient's genome was sequenced with the average depth of coverage 32.7× and mapped to the reference genome GRCh38. The WGS approach identified heterozygous missense variant *NOTCH3*(NM_000435.3):c.1320C>G p.(Cys440Trp) in exon 8 (NC_000019.10:g.15189047G>C). Targeted Sanger sequencing was done to confirm the presence of the variant; it was also performed on the patient's closest relatives – both parents and siblings (brother and sister) (Figure 3). Beside the patient, all family members were unaffected; the variant appeared de novo.

The identified variant was not reported in the Genome Aggregation Database (gnomAD v.3), 1000 Genomes, or in the polymorphism database dbSNP. No clinical information was available in ClinVar. The only information regarding variants in the same amino acid position (Cs440Ser and Cys440Gly) from the LOVD database were reported by Markus [14]. They were found in 2 individuals affected with CADASIL and interpreted as pathogenic on the basis of symptoms and familial cosegregation.
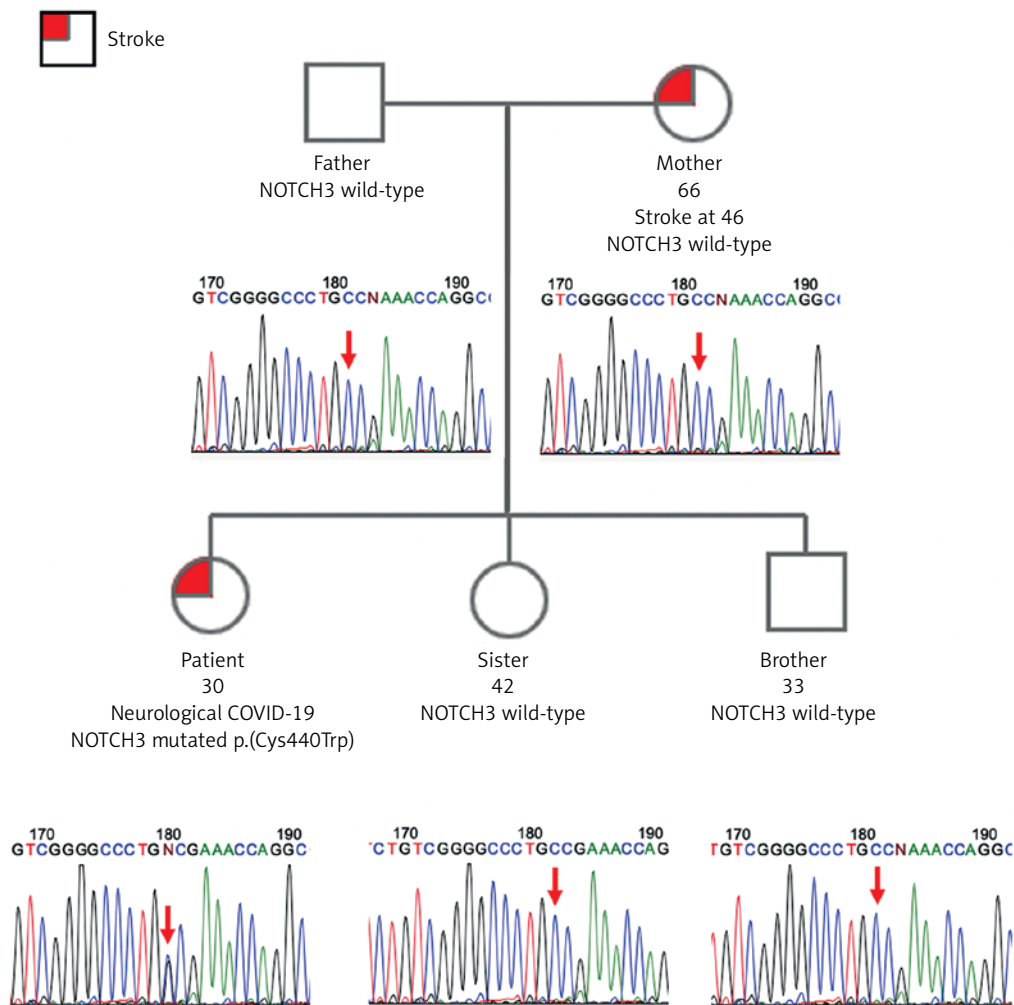
Figure 3. Pedigree of the patient's family. Affected individuals marked in red. The patient was analysed using the WGS approach and following targeted Sanger sequencing validation. All other family members were tested only with targeted Sanger sequencing. Corresponding electropherograms are located below each family member representation

The variant is located in the hot-spot region related to pathogenic mutations (all other known non-VUS missense/in-frame variants in this 51-nt long region were pathogenic). The identified variant was also evaluated to be deleterious/pathogenic by 11/12 online in silico prediction tools (based on pathogenic predictions from BayesDel_addAF, DEOGEN2, EIGEN, FATHMM-MKL, LIST-S2, M-CAP, MVP, MutationAssessor, MutationTaster, REVEL and SIFT vs only one benign prediction from PrimateAI) [15–26]. Pathogenicity was confirmed using ACMG/AMP guidelines (PS2, PM1, PM2, PM5, PP2, PP3, PP4) [27]. The identified variant in the *NOTCH3* gene allowed us to make the diagnosis of CADASIL.

In addition to the *NOTCH3* finding we registered a 4-fold lower level of blood mitochondrial DNA in the patient than the average of the Polish population (lower than the 3rd percentile). While the average blood mtDNA in our 890 healthy donor group was 79 copies per cell, the patient displayed only 20 genomes per diploid cell.

Although ADEM is thought to be a post-infectious disorder, the aetiology is still poorly understood. There was a single report on a mitochondrial genetic factor that could be the cause of ADEM in a paediatric patient. POLG – the nuclear gene coding a mitochondrial protein – was hypothesized to be causative or at least contribute to the disease [28].

The adult patient described in our report was not diagnosed with mitochondrial depletion syndrome as she displayed no clinical symptoms, apart from childhood-onset hemiparesis of unknown aetiology. As most congenital neurological syndromes that could have mimicked ADEM occur in children, we find it unlikely that such an encephalomyelitis type developed in an adult.

Nonetheless, we cannot exclude that a very mild mitochondrial depletion as well as NOTCH3 variant could have contributed to ADEM, which was triggered mainly by viral infection.

Methods and materials of whole genome sequencing

The integrity of the proband's isolated DNA was verified in 1% agarose gel. A library of 550 bp DNA fragments was prepared using the TruSeq DNA PCR Free kit (Illumina Inc, San Diego, CA, USA) and the quality of this library was examined using a 2100 Bioanalyzer (Agilent Technologies, Santa Clara, CA, USA). Next, 2 x 150 bp paired-end WGS was performed by Macrogen (Amsterdam, Netherlands), on the Illumina NovaSeq 6000 platform, yielding > 30× mean depth of coverage.

Data quality was assessed using FastQC v0.11.7 [14]. Reads were aligned to the GRCh38 reference genome using the Speedseq v0.1.2 toolkit [29] (BWA MEM 0.7.10 [30] alignment, Sambamba v0.5.9 [31] deduplication), and SNVs and indels identified by DeepVariant 0.8.0 software [32]. Copy number variants were called using CNVnator v0.4 [33]. All variants were annotated using Variant Effect Predictor [34], and analysis constrained to variants in a predefined set of 885 genes associated with neurological diseases (list available in supplementary material). SNVs with population frequency above 1% in the gnomAD population were excluded from the analysis. Resources used when assessing pathogenicity of candidate variants included: gnomAD v2.1.1 [35], dbSNP (153) [36], ClinVar [37], the Human Gene Mutation Database v2019.1 [38], OMIM [39], UniProt [40], KEGG v91.0 [41], and pathogenicity prediction scores such as SIFT [42], PolyPhen-2 [43] and CADD [44]. Targeted Sanger sequencing was performed on DNA samples of all family members subjected to genetic testing to confirm WGS results.

Results

Pathogenic variants in the *NOTCH3* gene were described as related to cerebral autosomal dominant arteriopathy with subcortical infarcts and leukoencephalopathy (CADASIL) – the most common inherited stroke disorder [45]. The clinical spectrum of the disease includes recurrent ischaemic episodes, progressive cognitive deficits, migraine and psychiatric disorders.

The *NOTCH3* gene encodes a single-pass transmembrane receptor containing 34 epidermal growth factor repeats (EGFr). Each EGFr is composed of approximately 40 amino acids, all containing 6 cysteine amino acids that form disulfide bridges [46]. *NOTCH3* mutations in CADASIL invariably lead to an uneven number of cysteines and disrupt normal disulfide bridge formation, causing misfolding of EGFr and increased *NOTCH3* multimerization [47]. This *NOTCH3* aggregation has a toxic effect on vascular smooth muscle cells. These changes lead to impaired cerebrovascular reactivity and decreased cerebral blood flow, believed to cause both chronic cerebral ischaemia and acute ischaemic events [48, 49]. Acute infection in the course of COVID-19 may stimulate inflammatory reactions, hypoxia and coagulopathy, which can additionally trigger ischaemic infarctions even in patients without classic vascular risk factors. A few patients with acute SARS-CoV-2 infection and CADASIL, who presented with multiple ischaemic infarcts, have recently been reported [50–52].

The identified variant p.(Cys440Trp) is located in EGFr 11, which has been related to a much milder phenotype and neurological symptoms occurring 12 years later than those with pathogenic variants located in EGFr [53].

Z.J. Król, M. Dorobek, M. Dąbrowski, J. Zielińska-Turek, B. Mruk, J. Walecki, K. Sklinda, R. Gil, A. Pawlak, M. Wojtaszewska, A. Lejman, P. Dobosz, P. Zawadzki, A. Pawłowska, M. Szczepaniak, D. Król, A. Zaczyński, W. Wierzba

Another interesting finding in our patient is the strikingly low level of mitochondrial DNA in the blood, below the 3rd percentile in the distribution of our reference healthy donor group. Several studies have shown the correlation between mtDNA blood levels and general fitness, risk of cardiovascular diseases and neurological functioning, especially in the elderly [54–56]. The low copy number of mtDNA in our proband could have been involved in the patient's condition, acting as a genetic modifier of the underlying condition. This finding may be at least partially responsible for the relatively early age of CADASIL onset and clinical display in the presented patient.

The simultaneous COVID-19 infection could probably provoke an exacerbation of a previously asymptomatic CADASIL patient and could lead to acute ischaemic multi-infarct encephalopathy, as the association between CADASIL and SARS-CoV-2 infection as a trigger mechanism has been described [50, 51, 57, 58]. There is also an association between CADASIL and influenza A infection. The infection can cause the appearance of new neurological symptoms [59]. Additionally, there is evidence suggesting that worsening of neurological symptoms can appear when treating migraine in CADASIL patients with anti-migraine drugs (e.g. drugs blocking CGRP), but this needs further investigation [60]. There are rare descriptions of the coexistence of autoimmunity in CADASIL patients which may possibly worsen clinical symptoms and signs [61].

Our patient developed symptoms of encephalopathy prior to clinical and radiological pulmonary symptoms. Moreover, the pulmonary symptoms during hospitalization were mild. The patient had radiologic features of pneumonia, which did not require any treatment other than high-flow oxygen therapy 20 l/min. The levels of IL-6 and other inflammatory markers outside the CNS were relatively low. The patient was initially treated with iv immunoglobulins, as the differential diagnosis included ADEM.

Many inflammatory and noninflammatory disorders can have similar clinical and radiologic features and should be considered in the differential diagnosis. Bacterial and viral inflammatory process were excluded (cerebrospinal fluid pleocytosis, the level of cerebrospinal fluid proteins and immunoglobulin index, gadolinium enhancement in MRI). Anti-MOG associated encephalomyelitis was also within the differential diagnosis. It was excluded due to the absence of anti-MOG antibodies. ADEM was suspected on the basis of clinical features and neuroimaging results. Magnetic resonance abnormalities in ADEM are frequently present in T2 weighted and fluid attenuated inversion recovery (FLAIR) sequences as non-uniform, poorly marginalized areas of increased signal intensity. They are usually large, multiple and asymmetric, and occur in subcortical and cortical areas. Periventricular white matter is also often involved. This correlated well with the radiological picture in our patient.

Thereafter the patient was administered convalescent plasma. Convalescent plasma, due to the high titre of SARS-CoV-2 neutralizing antibodies, is effectively used in the prevention and treatment of epidemic infections. These antibodies prevent the virus from entering the human cell by attacking one of the functional subunits of the S-glycoprotein, and therefore play a key role in direct virus neutralization. In the study by Tworek *et al.*, unlike in many other publications, shortened hospitalization was not observed in COVID-19 patients [13]. On the other hand, it was found that sufficiently early administered convalescent plasma may significantly reduce the development of acute respiratory failure and the need for mechanical ventilation.

Referring to the above, we suggest that the speed of disease progression, neurological deficits correlating with numerous diffuse changes in the brain imaging and the coexistence of preceding SARS-CoV-2 infection can lead to a hypothesis that this infection was responsible for the development of encephalopathy, with predominant white matter changes.

To improve the clarity of the results, a timeline of patient management (Figure 4) and a list of genes in the neurological panel (Table II) are presented.

Discussion

The diagnosis of white matter changes requires a broad approach combining sequential neuroimaging, clinical features, the course of the disease and laboratory data. White matter diseases affect the pattern of myelination and include a large diversity of acquired processes, e.g., autoimmune, infectious, vascular. These processes could play a role in the present case.

In our CADASIL patient, the restriction of diffusion of the lesions and its slow normalization over time could also suggest subcortical lacunar infarcts (Figure 1). However, this radiologic feature may also be present in ADEM associated with SARS-CoV-2 infection. Differential diagnosis between the two – ADEM and CADASIL – may be a great challenge [50], as it was in the present case.

One of the essential features of the white matter lesions' radiological assessment is the analysis of their distribution and evolution over time. Some studies have suggested that both anterior temporal lobe involvement and external capsule involvement are characteristic markers that may differentiate CADASIL from other diseases [62–64].

22.07.2020 – first symptoms – temperature elevated up to 37°C

25.07.2020 – anosmia

3.08.2020 – positive test for SARS-CoV-2

4.08.2020 – admission to the hospital

5.08.2020 – first MRI of the head

7.08.2020 – lumbar puncture; admission to anesthesiology and intensive care unit

7–9.08.2020 – infusion of immunoglobulins

8.08.2020 – control MRI

11–12.08.2020 – administration of convalescents' plasma

13.08.2020 – control MRI

16.08.2020 – resolution of the clinical symptoms

20.08 2020 – control MRI

3.09.2020 – follow-up MRI examination

5.11.2020 – final follow-up MRI examination

Figure 4. Timeline

Furthermore, the blood vessels of CADASIL patients are directly exposed to a variety of endogenous or exogenous inflammatory stimuli. Ling et al. analysed the expression levels of cytokines, chemokines and adhesion molecules in vascular smooth muscle cells (VSMC) and vascular endothelial cells (VEC) and TNF-α-induced inflammation was increased in both CADASIL VSMC and VEC. The ELISA assay further confirmed the upregulation of IL-6 protein in CADASIL VSMC and VEC culture medium in TNF-α-induced inflammation. In addition, they found increased adhesion of monocytes to CADASIL VEC in TNF-α-induced inflammation. Together, CADASIL VSMC and VEC showed higher sensitivity to inflammatory stimuli [26].

In addition, cytokine release in response to SARS-CoV-2 infection may lead to mild to severe clinical symptoms. Patients with severe conditions showed serum profiles with dramatically increased plasma levels of interleukins up to the state of "cytokine storm", including IL-6, IL-2, IL-7 and IL-10 [65]. In severely ill SARS patients, the concentrations of IFN-γ, IL-1, IL-6, IL-12, TGF-β, MCP-1 and IL-8 were higher than in patients with mild to moderate symptoms [66, 67]. Historically, IL-1β, IL-6 and IL-8 levels were also increased in patients with severe MERS-CoV infection [68].

With regard to the decreased level of IL-15, it is a critical immunoregulatory cytokine with antiviral properties [69]. IL-15 is expressed by bone marrow cells to help with T cell responses, acti-

vate NK cells, and modulate inflammation [70]. Deficiency of IL-15 has previously been shown to promote airway resistance in mice, while IL-15 inhibits pro-inflammatory cytokines, reduces goblet cell hyperplasia and regulates allergen-induced airway obstruction in mice by inducing interferon (IFN-γ) and IL-10-producing regulatory T cells [71].

In the present case, there were confluent white matter changes in the anterior temporal lobes and in the area of both external capsules (Figure 2). Similar localization of the lesions was described in another case recently reported by Zhang [49]. Some authors also emphasize the frequent location of the radiological changes in the upper frontal gyri, which is not present in our patient [64]. Other locations in which changes in the course of CADASIL syndrome may occur include the posterior temporal and occipital white matter, the basal ganglia, thalamus, internal capsule and the pons [64]. The involvement of the corpus callosum is a typical multiple sclerosis (MS) feature, could be present in ADEM and affects about 40% of patients with CADASIL [72]. The involvement of the corpus callosum is present in our case (Figure 5), but it was absent in the report of Zhang. In contrast, the occurrence of lesions in all infratentorial regions except the pons is unusual [49, 64, 72].

It has been suggested that white matter changes in ADEM should regress over time [73], while in our case the changes are still significant after 7 months of observation.

Z.J. Król, M. Dorobek, M. Dąbrowski, J. Zielińska-Turek, B. Mruk, J. Walecki, K. Sklinda, R. Gil, A. Pawlak, M. Wojtaszewska, A. Lejman, P. Dobosz, P. Zawadzki, A. Pawłowska, M. Szczepaniak, D. Król, A. Zaczyński, W. Wierzba

Table II. List of genes in the neurological panel

ABAT	CLN8	KCNT1	SLC6A1	FOLR1	PLP1	CHMP2B
ABCD1	CNTNAP2	KCTD7	SLC6A8	FOXG1	PNKP	DCTN1
ADAR	COL4A1	KDM5C	SLC9A6	FOXRED1	PNPO	FIG4
ADSL	COX15	KIF1A	SMS	GABRA1	POLG	FUS
AFG3L2	COX6B1	L2HGDH	SNAP25	GABRB2	POLR3A	GBE1
AGA	CPT2	LGI1	SNORD118	GABRB3	POLR3B	HEXA
AIFM1	CSF1R	LMNB1	SOX10	GABRG2	PPT1	HNRNPA1
AIMP1	CSTB	LRPPRC	SPATA5	GALC	PRICKLE1	KIAA0196
ALDH3A2	CTC1	LYRM7	SPTAN1	GAMT	PRIMA1	KIF5A
ALDH5A1	CTSD	MAGI2	ST3GAL3	GCDH	PRODH	OPTN
ALDH7A1	CTSF	MARS2	ST3GAL5	GCH1	PRRT2	PRF1
ALG13	CUL4B	MBD5	STX1B	GFAP	PSAP	REEP1
AMACR	CYP27A1	MECP2	STXBP1	GFM1	PTS	SETX
AMT	D2HGDH	MED12	SUMF1	GJC2	PURA	SLC52A2
AP4B1	DARS	MEF2C	SUOX	GLB1	PYCR2	SLC52A3
AP4E1	DARS2	MFSD8	SYN1	GLDC	QDPR	SOD1
AP4M1	DCX	MLC1	SYNGAP1	GLRB	RAB39B	SPAST
AP4S1	DDC	MOCS1	SYNJ1	GNAO1	RARS	SPG11
APOPT1	DEPDC5	MRPL44	SZT2	GNB1	RELN	SPG20
ARG1	DHFR	MTFMT	TAF1	GNE	RMND1	SQSTM1
ARHGEF9	DNAJC5	MTHFR	TBC1D24	GOSR2	RNASEH2A	TARDBP
ARSA	DNM1	MTOR	TBCD	GPHN	RNASEH2B	TUBA4A
ARX	DNM1L	NACC1	TBCE	GRIA3	RNASEH2C	UBQLN2
ASAH1	DOCK7	NDUFAF5	TBCK	GRIK2	RNASET2	VAPB
ASNS	DPYD	NDUFAF6	TBL1XR1	GRIN1	RNF216	VCP
ASPA	DPYS	NDUFS2	TCF4	GRIN2A	ROGDI	ADNP
ATP13A2	EARS2	NDUFS4	TPP1	GRIN2B	SAMHD1	BCL11A
ATP1A3	ECHS1	NDUFS7	TREX1	GRN	SCARB2	CACNA1C
ATRX	ECM1	NDUFS8	TSC1	GTPBP3	SCN1A	CNOT3
BRAT1	EEF1A2	NDUFV1	TSC2	HACE1	SCN1B	CNTN6
BTD	EFHC1	NECAP1	TTC19	HCN1	SCN2A	COL4A3BP
CACNA1A	EIF2B1	NEU1	TUBB4A	HECW2	SCN8A	CTNND2
CACNA1H	EIF2B2	NFU1	UBA5	HEPACAM	SCN9A	DHCR7
CACNB4	EIF2B3	NHLRC1	UBE2A	HIBCH	SCO1	EN2
CASK	EIF2B4	NOTCH3	UBE3A	HNRNPU	SDHAF1	FOXP1
CASR	EIF2B5	NRXN1	UNC80	HSD17B10	SERAC1	KMT5B
CC2D1A	EPM2A	NUBPL	VPS13A	HSPD1	SERPINI1	NLGN3
CDKL5	ETFA	OFD1	WDR26	HTRA1	SIK1	NLGN4X
CERS1	ETFB	OPHN1	WDR45	HTT	SLC12A5	NSD1
CHD2	ETFDH	PCDH19	WWOX	IBA57	SLC13A5	POGZ
CHRNA2	ETHE1	PGK1	YY1	IQSEC2	SLC19A3	PTCHD1

Table II. Cont.

CHRNA4	FA2H	PHF6	ZEB2	KCNA1	SLC25A1	PTEN
CHRNB2	FAM126A	PIGA	ZFYVE26	KCNA2	SLC25A15	RPL10
CLCN2	FAR1	PIGN	ALS2	KCNB1	SLC25A22	SHANK3
CLCN4	FARS2	PIGO	ANG	KCNC1	SLC2A1	TCF20
CLN3	FGF12	PIGT	ATL1	KCNH1	SLC35A2	TRIP12
CLN5	FH	PIGV	BSCL2	KCNQ2	SLC39A8	CCM2
CLN6	FLNA	PLCB1	CHCHD10	KCNQ3	SLC46A1	KRIT1
PDCD10	CDON	NDE1	TIMM8A	TRPV4	SLC16A2	EEF2
RASA1	FGF8	NHEJ1	TK2	UBA1	SMC1A	ELOVL4
ADCK3	FGFR1	PCNT	TMEM126A	ACSL4	SOX3	ELOVL5
ANO10	FOXH1	PHGDH	TUBB3	AFF2	SYP	FBXL4
APTX	GLI2	PLK4	TYMP	AP1S2	TSPAN7	FGF14
COQ2	GLI3	PQBP1	WFS1	ARHGEF6	UPF3B	FLVCR1
COQ4	NODAL	RARS2	DNAJC6	ATP6AP2	USP9X	FXN
COQ5	PTCH1	RTTN	FBXO7	BCOR	ZC4H2	GBA2
COQ6	SHH	SEPSECS	LRRK2	BRWD3	ZCCHC12	GRID2
COQ7	SIX3	STAMBP	PARK2	DDX3X	ZDHHC9	GRM1
COQ9	TGIF1	STIL	PARK7	DKC1	ZNF41	GSS
PDSS1	ZIC2	TSEN2	PDGFB	DLG3	ZNF674	HARS2
PDSS2	ACTB	TSEN54	PDGFRB	ELK1	ZNF711	INPP5E
SLC25A26	ACTG1	TUBGCP4	PINK1	FANCB	ZNF81	ITM2B
AGRN	ATP6V0A2	TUBGCP6	PLA2G6	FGD1	ABCB7	ITPR1
CHAT	FKTN	VRK1	PRKRA	FMR1	ABHD12	KCNC3
CHRNA1	ISPD	WDR62	SLC20A2	FTSJ1	AHI1	KCND3
CHRNB1	KATNB1	WDR73	SLC6A3	GDI1	ARL13B	KCNJ10
CHRND	LAMB1	XRCC4	SPR	GK	ARL6	KIF1C
CHRNE	LARGE	ACO2	TH	GPC3	ATCAY	KIF7
CHRNG	PAFAH1B1	ANTXR1	VPS35	HCCS	ATM	LAMA1
COLQ	POMGNT2	C10ORF2	ADGRG1	HPRT1	ATP8A2	LARS2
DOK7	POMT1	C12ORF65	GPSM2	HUWE1	BBS1	MKKS
DPAGT1	TUBA1A	CHN1	KIF1BP	IDS	BBS10	MKS1
FLAD1	TUBB2B	CISD2	LAMC3	IGBP1	BBS12	MME
GFPT1	TUBG1	FDXR	NSDHL	IL1RAPL1	BBS2	MTPAP
LAMB2	VLDLR	FRMD7	OCLN	KIAA2022	BBS4	MTTP
MUSK	YWHAE	GPR143	RAB18	KLF8	BBS5	NOL3
PLEC	AKT3	HESX1	SRPX2	L1CAM	BBS7	NPHP1
RAPSN	AMPD2	KIF21A	TUBA8	LAMP2	BBS9	PDYN
SCN4A	ASPM	MFN2	TUBB2A	MAGT1	BEAN1	PEX7
STIM1	ATR	NDUFS1	AARS	MAOA	C5ORF42	PHYH
ABCA7	CDK5RAP2	NR2F1	ATP7A	MBTPS2	CA8	PNKD
APOE	CENPF	OPA1	BICD2	MID1	CAMTA1	PNPLA6

Z.J. Król, M. Dorobek, M. Dąbrowski, J. Zielińska-Turek, B. Mruk, J. Walecki, K. Sklinda, R. Gil, A. Pawlak, M. Wojtaszewska, A. Lejman,
P. Dobosz, P. Zawadzki, A. Pawłowska, M. Szczepaniak, D. Król, A. Zaczyński, W. Wierzba

Table II. Cont.

APP	CENPJ	OPA3	DNAJB2	MTM1	CAPN1	PPP2R2B
MAPT	CEP152	OTX2	EXOSC8	NDP	CC2D2A	PRKCG
PRNP	CEP63	PAX6	FBXO38	NDUFA1	CCDC88C	RPGRIP1L
PSEN1	DYNC1H1	PHOX2A	GARS	NHS	CEP290	RUBCN
PSEN2	DYRK1A	PRPS1	HSPB1	NXF5	CEP41	SACS
SIGMAR1	EFTUD2	ROBO3	HSPB3	OCRL	CLPP	SIL1
SNCA	EXOSC3	RRM2B	HSPB8	OTC	COASY	SLC1A3
SORL1	KANSL1	RTN4IP1	IGHMBP2	PAK3	COX20	SNX14
TREM2	KIF11	SALL4	LAS1L	PDHA1	CP	SPTBN2
DMD	LIG4	SLC25A4	PLEKHG5	PHF8	CWF19L1	STUB1
EMD	MCPH1	SLC25A46	SCO2	PORCN	CYP2U1	SYNE1
FHL1	MFSD2A	SLC38A8	SLC5A7	RBM10	DNAJC19	SYT14
LMNA	MRE11A	SOX2	SMN1	RPS6KA3	DNMT1	TCTN1
TMEM43	MYCN	SPG7	SMN2	SHROOM4	EBF3	TCTN2
TCTN3	MARS	FLNC	DHCR24	CACNA1S		
TDP1	MCM3AP	GAA	DIS3L2	CLCN1		
TGM6	MED25	GMPPB	DNMT3A	KCNJ2		
TMEM138	MPZ	ITGA7	EED	ALAD		
TMEM216	MTMR2	KBTBD13	EZH2	ALAS2		
TMEM231	MYOT	KLHL40	KPTN	CPOX		
TMEM237	NDRG1	KLHL41	MPDZ	FECH		
TMEM240	NEFH	LAMA2	NFIX	HFE		
TMEM67	NEFL	LIMS2	PIK3CA	HMBS		
TRIM32	NGF	LMOD3	PIK3R2	PPOX		
TTBK2	NTRK1	MEGF10	RNF135	UROD		
TTC8	PDK3	MICU1	SETD2	UROS		
TTPA	PMP22	MYH7	ACAD9	B4GALNT1		
VAMP1	PRDM12	NEB	ACADL	C19ORF12		
WDPCP	PRX	PABPN1	ACADM	CTNNB1		
WDR81	RAB7A	PNPLA2	ACADVL	CYP7B1		
ZNF423	SBF1	POGLUT1	AGL	DDHD1		
ARHGEF10	SBF2	RBCK1	AHCY	DDHD2		
ATAD3A	SCN11A	SELENON	ALDOA	NIPA1		
ATL3	SEP9	SGCA	AMPD1	PAH		
BAG3	SH3TC2	SGCB	ENO3			
CCT5	SLC12A6	SGCD	GYG1			
COX10	SMAD3	SGCG	GYS1			
COX6A1	SPTLC1	SMCHD1	HADHA			
CTDP1	SPTLC2	SPEG	ISCU			
DCAF8	SURF1	TCAP	LDHA			
DHTKD1	TFG	TMEM126B	LPIN1			

Table II. Cont.

DNM2	TRIM2	TNNT1	MYH3
DST	TTR	TNPO3	PFKM
EGR2	WNK1	TOR1AIP1	PGAM2
FAM134B	YARS	TPM2	PGM1
FBLN5	COL12A1	TPM3	PHKA1
FGD4	COL4A2	TRAPPC11	POLG2
GAN	COL6A1	VMA21	PYGM
GDAP1	COL6A2	GATM	RYR1
GJB1	COL6A3	ADCY5	SLC22A5
GNB4	ACTA1	ANO3	SLC25A20
HADHB	ANO5	BCAP31	SUCLA2
HARS	ATP2A1	DCAF17	TANGO2
HINT1	B3GALNT2	GNAL	ATP1A2
HK1	CAPN3	KMT2B	KCNK18
IKBKAP	CAV3	SGCE	ARFGEF2
INF2	CFL2	THAP1	EMX2
KARS	CRYAB	TOR1A	FAT4
KIF1B	DES	AKT1	FLVCR2
LDB3	DNAJB6	CCND2	RAB3GAP1
LITAF	DYSF	CDKN1C	RAB3GAP2
LRSAM1	FKRP	CHD8	TMEM5
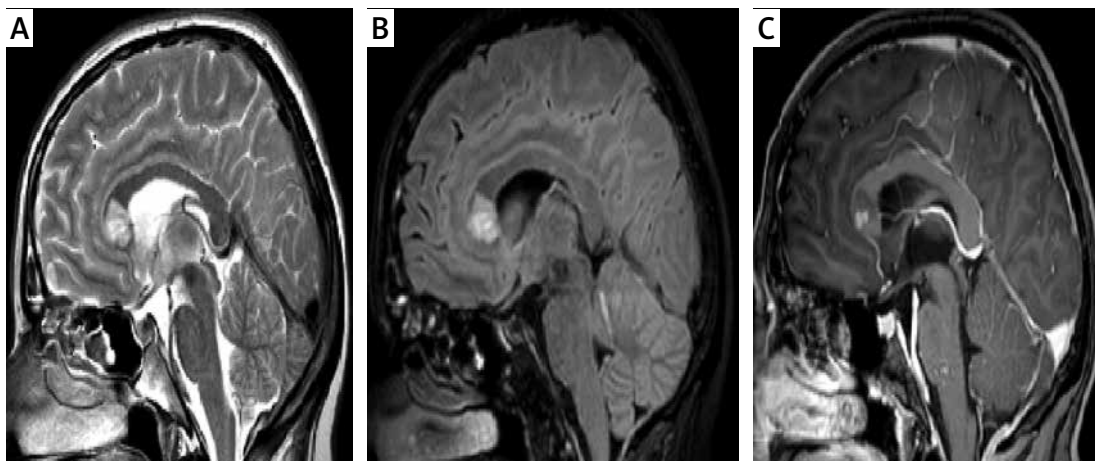
Figure 5. The lesion in the genu of the corpus callosum shows high signal intensity on T2 WI (**A**) and FLAIR (**B**) and punctate enhancement after intravenous contrast administration (**C**)

Although absent in our case, microbleeds may occur in 30–70% of CADASIL patients, and their frequency of occurrence increases with patient's age; intracerebral haemorrhage have also been described in a number of patients [5, 74, 75]. Our patient was only 30 years old and did not have any vascular risk factors.

Contrast enhancement present in the acute phase of the disease does not significantly narrow the differential diagnosis and may occur in many white matter diseases [72].

Subcortical lacunar infarcts on a background of chronic microangiopathic ischaemic changes, and white matter of the anterior temporal poles, superior frontal lobes, and external capsules are typically affected. These are the key diagnostic features of CADASIL, present in our patient.

Z.J. Król, M. Dorobek, M. Dąbrowski, J. Zielińska-Turek, B. Mruk, J. Walecki, K. Sklinda, R. Gil, A. Pawlak, M. Wojtaszewska, A. Lejman,
P. Dobosz, P. Zawadzki, A. Pawłowska, M. Szczepaniak, D. Król, A. Zaczyński, W. Wierzba

In spite of *de novo* origin of the identified *NOTCH3* variant in the patient, the patient's mother suffered an early stroke episode at the age of 46. The event was not related to COVID-19 and she had no other predisposing conditions. The phenocopy could be uncorrelated to the proband's CADASIL; other unknown, potentially female-specific, genetic factors could cause neurological conditions; or there could be an obscured mosaicism in the mother. Notably, Markus et al. reported that 19.5% of tested individuals, in whose families CADASIL occurred, suffered an ischaemic stroke but did not harbour the pathogenic mutations [14].

Recently, it has been shown that CADASIL pathogenic variants may occur in 1 : 300 individuals in the general population [49]. This frequency is higher than the minimal estimated CADASIL prevalence, which means that CADASIL may be underdiagnosed. It could be suggested that a number of pathogenic mutations in the population are associated with milder phenotype or are non-penetrant. The awareness of a potentially high number of asymptomatic CADASIL individuals in the population may have important implications for the diagnosis and treatment of patients with neurological symptoms related to COVID-19 and other acute infections. Determining the process which causes ischaemic infarcts in CADASIL patients with COVID-19 could enable appropriate measures of prevention to be applied in the foreseeable future.

In conclusion, this case underlines diagnostic difficulties associated with making the proper diagnosis as the clinical features and radiologic findings may be similar in a number of different entities. The proper diagnosis is of paramount importance as it can lead to applying successful treatment. The diagnostic process undertaken in this study strongly supports the value of widespread use of WGS, as it can contribute in future to lowering the number of undiagnosed CADASIL patients and therefore resolve the problem of underdiagnosing CADASIL in the general population. The same could be said about other underdiagnosed health conditions with underlying genetic factors, which were not a part of this study.

Conflict of interest

The authors declare no conflict of interest.

References

1. Ramos-Araque ME, Siegler JE, Ribo M, et al. Stroke etiologies in patients with COVID-19: the SVIN COVID-19 multinational registry. BMC Neurology 2021; 21: 43.
2. al Mazrouei SS, Saeed GA, al Helali AA, et al. COVID-19-associated encephalopathy: nurological manifestation of COVID-19. Radiol Case Rep 2020; 15: 1646-9.
3. Kremer S, Lersy F, de Sèze J, et al. Brain MRI findings in severe COVID-19: a retrospective observational study. Radiology 2020; 297: E242-51.
4. Novi G, Rossi T, Pedemonte E, et al. Acute disseminated encephalomyelitis after SARS-CoV-2 infection. Neurol Neuroimmunol Neuroinflamm 2020; 7: e797.
5. Muccioli L, Pensato U, Cani I, et al. COVID-19-associated encephalopathy and cytokine-mediated neuroinflammation. Ann Neurol 2020; 88: 860-1.
6. Beyrouti R, Adams ME, Benjamin L, et al. Characteristics of ischaemic stroke associated with COVID-19. J Neurol Neurosurg Psychiatry 2020; 91: 889-91.
7. Mao L, Jin H, Wang M, et al. Neurologic manifestations of hospitalized patients with coronavirus disease 2019 in Wuhan, China. JAMA Neurol 2020; 77: 683-90.
8. Chen N, Zhou M, Dong X, et al. Epidemiological and clinical characteristics of 99 cases of 2019 novel coronavirus pneumonia in Wuhan, China: a descriptive study. Lancet 2020; 395: 507-13.
9. Tournier-Lasserve E. New players in the genetics of stroke. N Engl J Med 2002; 347: 1711-2.
10. Joutel A, Corpechot C, Ducros A, et al. Notch3 mutations in CADASIL, a hereditary adult-onset condition causing stroke and dementia. Nature 1996; 383: 707-10.
11. Ruchoux MM, Maurage CA. CADASIL. J Neuropathol Exp Neurol 1997; 56: 947-64.
12. Chabriat H, Joutel A, Dichgans M, et al. CADASIL. Lancet Neurol 2009; 8: 643-53.
13. Tworek A, Jaroń K, Uszyńska-Kałuża B, et al. Convalescent plasma treatment is associated with lower mortality and better outcomes in high-risk COVID-19 patients: propensity-score matched case-control study. Int J Infect Dis 2021; 105: 209-15.
14. Markus HS, Martin RJ, Simpson MA, et al. Diagnostic strategies in CADASIL. Neurology 2002; 59: 1134-8.
15. Raimondi D, Tanyalcin I, Ferté J, et al. DEOGEN2: prediction and interactive visualization of single amino acid variant deleteriousness in human proteins. Nucleic Acids Research 2017; 45: W201-6.
16. Ionita-Laza I, McCallum K, Xu B, et al. A spectral approach integrating functional genomic annotations for coding and noncoding variants. Nat Genet 2016; 48: 214-20.
17. Shihab HA, Rogers MF, Gough J, et al. An integrative approach to predicting the functional effects of non-coding and coding sequence variation. Bioinformatics 2015; 31: 1536-43.
18. Malhis N, Jacobson M, Jones SJM, et al. LIST-S2: taxonomy based sorting of deleterious missense mutations across species. Nucleic Acids Res 2020; 48: W154-61.
19. Jagadeesh KA, Wenger AM, Berger MJ, et al. M-CAP eliminates a majority of variants of uncertain significance in clinical exomes at high sensitivity. Nat Genet 2016; 48: 1581-6.
20. Qi H, Zhang H, Zhao Y, et al. MVP predicts the pathogenicity of missense variants by deep learning. Nat Commun 2021; 12: 510.
21. Reva B, Antipin Y, Sander C. Predicting the functional impact of protein mutations: application to cancer genomics. Nucleic Acids Res 2011; 39: e118.
22. Schwarz JM, Cooper DN, Schuelke M, et al. MutationTaster2: mutation prediction for the deep-sequencing age. Nature Methods 2014; 11: 361-2.
23. Ioannidis NM, Rothstein JH, Pejaver V, et al. REVEL: an ensemble method for predicting the pathogenicity of rare missense variants. Am J Human Genetics 2016; 99: 877-85.

24. Sundaram L, Gao H, Padigepati SR, et al. Predicting the clinical impact of human mutation with deep neural networks. Nature Genet 2018; 50: 1161-70.

25. Kumar P, Henikoff S, Ng PC. Predicting the effects of coding non-synonymous variants on protein function using the SIFT algorithm. Nature Protocols 2009; 4: 1073-81.

26. Ling C, Liu Z, Song M, et al. Modeling CADASIL vascular pathologies with patient-derived induced pluripotent stem cells. Protein Cell 2019; 10: 249-71.

27. Richards S, Aziz N, Bale S, et al. Standards and guidelines for the interpretation of sequence variants: a joint consensus recommendation of the American College of Medical Genetics and Genomics and the Association for Molecular Pathology. Genet Med 2015; 17: 405-24.

28. Harris MO, Walsh LE, Hattab EM, et al. Is It ADEM, POLG, or Both? Arch Neurol 2010; 67: 493-6.

29. Andrews S. https://www.bioinformatics.babraham.ac.uk/projects/fastqc/, https://www.bioinformatics.babraham.ac.uk/projects/fastqc/ (accessed August 17, 2021).

30. Chiang C, Layer RM, Faust GG, et al. SpeedSeq: ultra-fast personal genome analysis and interpretation. Nature Methods 2015; 12: 966-8.

31. Li H. Aligning sequence reads, clone sequences and assembly contigs with BWA-MEM. Preprint Genomix 2013. arXiv:1303.3997.

32. Tarasov A, Vilella AJ, Cuppen E, et al. Sambamba: fast processing of NGS alignment formats. Bioinformatics 2015; 31: 2032-4.

33. Poplin R, Chang PC, Alexander D, et al. A universal SNP and small-indel variant caller using deep neural networks. Nature Biotechnol 2018; 36: 983-7.

34. Abyzov A, Urban AE, Snyder M, et al. CNVnator: an approach to discover, genotype, and characterize typical and atypical CNVs from family and population genome sequencing. Genome Res 2011; 21: 974-84.

35. McLaren W, Gil L, Hunt SE, et al. The Ensembl Variant Effect Predictor. Genome Biol 2016; 17: 122.

36. National Center for Biotechnology Information; http://www.ncbi.nlm.nih.gov/projects/SNP/ (accessed August 17, 2021).

37. National Center for Biotechnology Information; https://www.ncbi.nlm.nih.gov/clinvar/ (accessed August 17, 2021).

38. Human Gene Mutation Database; http://www.hgmd.cf.ac.uk/ac/index.php (accessed August 17, 2021).

39. Online Mendelian Inheritance in Man; https://www.omim.org/ (accessed August 17, 2021).

40. Scientific community with a comprehensive; https://www.uniprot.org/ (accessed August 17, 2021).

41. Kyoto Encyclopedia of Genes and Genomes; https://www.genome.jp/kegg/ (accessed August 17, 2021).

42. Sim NL, Kumar P, Hu J, et al. SIFT web server: predicting effects of amino acid substitutions on proteins. Nucleic Acids Research 2012; 40: W452-7.

43. Adzhubei IA, Schmidt S, Peshkin L, et al. A method and server for predicting damaging missense mutations. Nature Methods 2010; 7: 248-9.

44. Pless ML, Chen YB, Copen WA, et al. Case 9-2010. N Engl J Med 2010; 362: 1129-38.

45. Gravesteijn G, Hack RJ, Opstal AM van, et al. Eighteen-year disease progression and survival in CADASIL. J Stroke 2021; 23: 132-4.

46. Rutten JW, Haan J, Terwindt GM, et al. Interpretation of NOTCH3 mutations in the diagnosis of CADASIL. Exp Rev Mol Diagnostics 2014; 14: 593-603.

47. Pfefferkorn T, von Stuckrad-Barre S, Herzog J, et al. Reduced cerebrovascular CO_2 reactivity in CADASIL. Stroke 2001; 32: 17-21.

48. Tuominen S, Miao Q, Kurki T, et al. Positron emission tomography examination of cerebral blood flow and glucose metabolism in young CADASIL patients. Stroke 2004; 35: 1063-7.

49. Zhang T, Hirsh E, Zandieh S, et al. COVID-19-associated acute multi-infarct encephalopathy in an asymptomatic CADASIL patient. Neurocritical Care 2021; 34: 1099-102.

50. Trifan G, Hillmann M, Testai FD. Acute stroke as the presenting symptom of SARS-CoV-2 infection in a young patient with cerebral autosomal dominant arteriopathy with subcortical infarcts and leukoencephalopathy. J Stroke Cerebrovasc Dis 2020; 29: 105167.

51. Williams OH, Mohideen S, Sen A, et al. Multiple internal border zone infarcts in a patient with COVID-19 and CADASIL. J Neurol Sci 2020; 416: 116980.

52. Rutten JW, van Eijsden BJ, Duering M, et al. The effect of NOTCH3 pathogenic variant position on CADASIL disease severity: NOTCH3 EGFr 1–6 pathogenic variant are associated with a more severe phenotype and lower survival compared with EGFr 7–34 pathogenic variant. Genet Med 2019; 21: 676-82.

53. Castellani CA, Longchamps RJ, Sun J, et al. Thinking outside the nucleus: mitochondrial DNA copy number in health and disease. Mitochondrion 2020; 53: 214-23.

54. Mengel-From J, Thinggaard M, Dalgård C, et al. Mitochondrial DNA copy number in peripheral blood cells declines with age and is associated with general health among elderly. Human Genet 2014; 133: 1149-59.

55. Filograna R, Mennuni M, Alsina D, et al. Mitochondrial DNA copy number in human disease: the more the better? FEBS Lett 2021; 595: 976-1002.

56. Auer DP, Pütz B, Gössl C, et al. Differential lesion patterns in CADASIL and sporadic subcortical arteriosclerotic encephalopathy: MR imaging study with statistical parametric group comparison. Radiology 2001; 218: 443-51.

57. Rajendran I, Natarajan MD, Narwani P, et al. A case of cerebral autosomal dominant arteriopathy with subcortical infarcts and leukoencephalopathy (CADASIL) presenting as post-infectious manifestation of SARS-CoV-2 infection. BJR Case Rep 2021; 7: 20210020.

58. Mizutani K, Sakurai K, Mizuta I, et al. Multiple border-zone infarcts triggered by influenza a virus infection in a patient with cerebral autosomal dominant arteriopathy presenting with subcortical infarcts and leukoencephalopathy. J Stroke Cerebrovasc Dis 2020; 29: 104701.

59. de Boer I, MaassenVanDenBrink A, Terwindt GM. The potential danger of blocking CGRP for treating migraine in CADASIL patients. Cephalalgia 2020; 40: 1676-8.

60. Paraskevas GP, Bougea A, Synetou M, et al. CADASIL and autoimmunity: coexistence in a family with the R169C mutation at exon 4 of the NOTCH3 Gene. Cerebrovasc Dis 2014; 38: 302-7.

61. Feng BJ. PERCH: a unified framework for disease gene prioritization. Human Mutation 2017; 38: 243-51.

62. O'Sullivan M, Jarosz JM, Martin RJ, et al. MRI hyperintensities of the temporal lobe and external capsule in patients with CADASIL. Neurology 2001; 56: 628-34.

63. Singhal S, Rich P, Markus HS. The spatial distribution of mr imaging abnormalities in cerebral autosomal dominant arteriopathy with subcortical infarcts and leukoencephalopathy and their relationship to age and clinical features. Am J Neuroradiol 2005; 26: 2481-7.

64. Sarbu N, Shih RY, Jones R, et al. White matter diseases with radiologic-pathologic correlation. Radio Graphics 2016; 36: 1426-47.

Z.J. Król, M. Dorobek, M. Dąbrowski, J. Zielińska-Turek, B. Mruk, J. Walecki, K. Sklinda, R. Gil, A. Pawlak, M. Wojtaszewska, A. Lejman, P. Dobosz, P. Zawadzki, A. Pawłowska, M. Szczepaniak, D. Król, A. Zaczyński, W. Wierzba

65. Zumla A, Hui DS, Azhar EI, et al. Reducing mortality from 2019-nCoV: host-directed therapies should be an option. Lancet 2020; 395: e35-6.

66. Chien JY, Hsueh PR, Cheng WC, et al. Temporal changes in cytokine/chemokine profiles and pulmonary involvement in severe acute respiratory syndrome. Respirology 2006; 11: 715-22.

67. Zhang Y, Li J, Zhan Y, et al. Analysis of serum cytokines in patients with severe acute respiratory syndrome. Infect Immun 2004; 72: 4410-5.

68. Lau SKP, Lau CCY, Chan KH, et al. Delayed induction of proinflammatory cytokines and suppression of innate antiviral response by the novel Middle East respiratory syndrome coronavirus: implications for pathogenesis and treatment. J General Virol 2013; 94: 2679-90.

69. Verbist KC, Klonowski KD. Functions of IL-15 in anti-viral immunity: multiplicity and variety. Cytokine 2012; 59: 467-78.

70. Kandikattu HK, Upparahalli Venkateshaiah S, Mishra A. Synergy of Interleukin (IL)-5 and IL-18 in eosinophil mediated pathogenesis of allergic diseases. Cytokine Growth Factor Rev 2019; 47: 83-98.

71. Venkateshaiah SU, Zhu X, Rajavelu P, et al. Regulatory effects of IL-15 on allergen-induced airway obstruction. J Allergy Clin Immunol 2018; 141: 906-17.

72. Guimarães MPM, Nascimento ACB, Alvarenga RMP. CLINICAL course of acute disseminated encephalomyelitis in adults from Rio de Janeiro: retrospective study of 23 cases and literature review. Multiple Sclerosis Related Disord 2020; 46: 102424.

73. Lesnik Oberstein SAJ, van den Boom R, van Buchem MA, et al. Cerebral microbleeds in CADASIL. Neurology 2001; 57: 1066-70.

74. Rinnoci V, Nannucci S, Valenti R, et al. Cerebral hemorrhages in CADASIL: report of four cases and a brief review. J Neurol Sci 2013; 330: 45-51.

75. Rutten JW, Dauwerse HG, Gravesteijn G, et al. Archetypal NOTCH3 mutations frequent in public exome: implications for CADASIL. Ann Clin Transl Neurol 2016; 3: 844-53.